Experimental determination of the solubility product of dolomite at 50 to 175 °C

Pascale Bénézeth[1]*, Ulf-Niklas Berninger[1,2], Nico Bovet[3], Jacques Schott[1] and Eric H. Oelkers[1,4]

[1] *Géosciences Environnement Toulouse, GET – CNRS – IRD – OMP – Université de Toulouse, 14, Avenue Edouard Belin, 31400 Toulouse, France*

[2] *Dept. für Geo- und Umweltwissenschaften, Ludwig-Maximilians-Universität München, Theresienstr. 41, 80333 München, Germany.*

[3] *University of Copenhagen*

[4] *Department of Earth Sciences, UCL, Gower Street, WC1E 6BT London, United Kingdom.*

***Corresponding author:**

Tel.: +33 5 61 33 25 85; fax: +33 5 61 33 25 60

E-mail address: pascale.benezeth@get.omp.eu

Abstract

The solubility of natural dolomite was investigated from 50 to 175 °C in 0.1 mol/kg NaCl solutions using a hydrogen electrode concentration cell (HECC). The resulting apparent solubility products ($Q_{sp\text{-}dol}$) for the reaction

$$Dolomite = Ca^{2+} + Mg^{2-} + 2\ CO_3^{2-}$$

were extrapolated to infinite dilution to generate the equilibrium constants for this reaction ($K_{sp°\text{-}dol}$),. Retrieved equilibrium constants are based on a constant standard state isobaric heat capacity ($\Delta_r C_p^o$) of -789.832 J/mol/K for this dolomite hydrolysis reaction and can be accurately described using

$$\log_{10} K_{sp°\text{-}mgs} = a + b/T\ (\mathrm{K}) + cT\ (\mathrm{K}),$$

where a = 18.1777, b = -4400.8736 K and $c_{(fixed)}$= -0.06919 K^{-1}. Resulting constants are nearly equal to those determined from SUPCRT92 (Johnson et al., 1992) at 200 C, but as much as 1.8 orders of magnitude more negative at 50 °C, suggesting that dolomite is somewhat more stable than previously assumed. Standard equilibrium constants generated in this study were used together with corresponding properties for the aqueous species to calculate revised standard state thermodynamic properties for dolomite.

Keywords: dolomite solubility product, dolomite thermodynamic properties

1. Introduction.

Dolomite, $CaMg(CO_3)_2$ is a double carbonate in which Mg^{2+} and Ca^{2+} are segregated into separate planes of the crystal structure (Antao et al., 2004; Lippmann, 1973). It is a common mineral in sedimentary rocks, ubiquitous in the past, yet rarely precipitates in modern environments (Arvidson and MacKenzie, 1999). Stoichiometric dolomite, also called "ordered", "ideal" or "primary" dolomite (as opposed to disordered or protodolomite) is also difficult to synthesize in the laboratory (Usdowski, 1994). The uncertainties surrounding dolomite precipitation mechanisms are commonly referred to as the "dolomite problem"; this dolomite problem has attracted the attention of scientists for more than a century (c.f. Arvidson and MacKenzie, 1999; Land, 1998).

Due to the difficulty precipitating dolomite in the laboratory, questions surrounding its crystallinity and other experimental challenges including controlling experimental CO_2 partial pressure and the measurement of pH and alkalinity measurements above ambient temperature, there is a wide disparity of dolomite solubility products available in the literature. This study is aimed to resolve this disparity through the measurement of natural dolomite solubility from 50 to 175 °C. Taking advantage of the hydrogen electrode concentration cell, we have verified the congruent dissolution of dolomite during our experiments and have constrained its solubility via both dissolution and precipitation. The purpose of this study is to report the results of this effort and to present a revised setoff consistent thermodynamics data for dolomite solubility as a function of temperature.

2. Summary of past work

The standard state adopted in this study for all thermodynamic calculations is that of unit activity for pure minerals and H_2O at any temperature and pressure. For aqueous species other than H_2O, the standard state is unit activity of the species in a hypothetical 1 molal solution referenced to infinite dilution at any temperature and pressure.

Dolomite dissolution and precipitation can be described by the reaction

$$CaMg(CO_3)_2 = Ca^{2+} + Mg^{2+} + 2CO_3^{2-} \quad (1),$$

The law of mass action for reaction 1 can be written as

$$K_{sp°-dol} = a_{Ca^{2+}} a_{Mg^{2+}} \left(a_{CO_3^{2-}}\right)^2$$

where $K_{sp°\text{-}dol}$ denotes the equilibrium constant for reaction (1) and a_i refers to the activity of the subscripted aqueous species. Due to a variety of experimental challenges there is much disparity in the equilibrium constants for reaction (1) reported in the literature. For example, experimentally determined equilibrium constants obtained at 25 °C in pure water and 1 bar pCO_2 range from -16.5 to -19.35 (see Table 1; Garrels *et al.*, 1960; Halla and Van Tassel, 1965; Yanat'yeva, 1952). Yanat'eva (1952) reported a $\log_{10} K_{sp°\text{-}dol}$ of -18.37 at 25 °C, measured from dolomite dissolution experiments performed in pure water performed over 100 days. Garrels *et al.* (1960) performed dolomite dissolution experiments in pure water at 25 °C and 1 atm pCO_2 for 18h. The pH at equilibrium between aqueous solution and <0.1 mm dolomite grains was measured as 5.68±0.02. These results yield a $\log_{10} K_{sp°\text{-}dol}$ value of -19.34. However, Garrels *et al.* (1960) reported that adding well-ground dolomite powder to their experimental solutions when they were close to the equilibrium pH of ~5.6 resulted in a rapid increase of pH to 6.2. This latter result yields a $\log_{10} K_{sp°\text{-}dol}$ value of -16.44, which may indicate failure to reach equilibrium. Langmuir (1964) performed dolomite dissolurion experiments in distilled water and dilute $MgCl_2$ solutions. Halla and Van Tassel (1965) reported a $\log_{10} K_{sp°\text{-}dol}$ of -17.76 at 21 °C. More recently, Sherman and Barak (2000) performed dolomite dissolution experiments at 25 °C and in Ca-Mg-HCO_3/CO_3 solutions for almost 2 years and derived a mean $\log_{10} K_{sp°\text{-}dol}$ value of -17.2±0.2, which is in agreement with that calculated from the thermodynamic properties of dolomite reported by Robie *et al.* (1978)

($\log_{10} K_{sp°\text{-dol}}$ = -17.12), as can be seen in Figure 1, where most of the $\log_{10} K_{sp°\text{-dol}}$ values gathered in Table 1 are illustrated as a function of the reciprocal temperature including the values generated from SUPCRT92 (Johnson et al., 1992).

Table 1. Equilibrium constant for the dolomite solubility reaction (1) obtained from experiments and/or thermodynamic calculations reported in the literature.

T (°C)	$\log_{10} K_{sp°\text{-dol}}$	Conditions/Notes	Reference
25	-18.37	dissolution in pure water, 1 atm p_{CO2} for 100 days	Yanat'eva (1952)
25	-16.8	dissolution in artificial seawater (35‰) atmospheric CO_2	Kramer (1959)
25	-19.34	dissolution in in pure water and 1 atm p_{CO2} for 18 hours	Garrels *et al.* (1960)
25	-16.44	added well-grounded dolomite to the above experiment	Garrels *et al.* (1960)
22-27	-16.70	Assumed groundwater in equilibrium with dolomite	Hsu (1963)
25 (?)	-16.54	Assumed groundwater in equilibrium with dolomite	Barnes and Back (1964)
25	-17.0	dissolution in distilled water and dilute $MgCl_2$ solutions	Langmuir (1964)
21	-17.76	dissolution in pure water, 1 atm p_{CO2} for 546 days	Halla and Van Tassel (1965)
25	-17.12	Calculated	Robie *et al.* (1978)
25	-18.20	calculated from HCl solution calorimetry at 85°C	Navrotsky and Capobianco (1987)
25	-18.15	calculated based on phase equilibria by Helgeson et al. (1978)	Johnson *et al.* (1992) (SUPCRT92)
25	-17.09±0.37	calculated from HCl solution 300.15K	Hemingway and Robie (1994)
25	-17.20	dissolution in in Ca-Mg-HCO_3/CO_3 solutions for ~2 years	Sherman and Barak (2000)
80	-17.95	dissolution in HCl-$NaHCO_3$ solutions	Gautelier *et al.* (2007)

The $\log_{10} K_{sp°\text{-dol}}$ values reported by Halla and Van Tassel (1965) and Yanat'eva (1952) fall between a group of measurements that obtained values near -17.00 (Robie *et al.*, 1978) and retrieved from HCl solution calorimetry experiments performed at 85 °C by Navrotsky and Capobianco (1987). The SUPCRT92 database uses dolomite thermodynamic data from Helgeson *et al.* (1978) to calculate this equilibrium constant. These data are based on phase equilibrium for the reaction:

4 talc + 5 dolomite = 5 diopside + 6 forsterite + 10 CO_2 + 4 H_2O,

at P = 2 kbar and temperatures ranging from 400-600 °C.

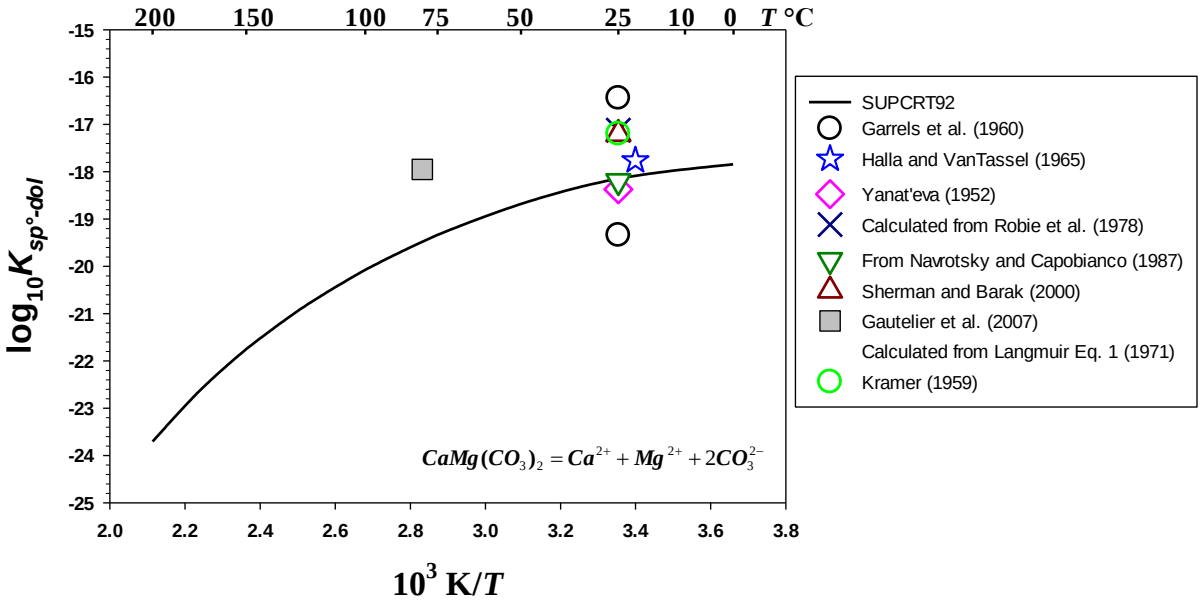

Figure 1: Summary of dolomite solubility products constants reported in the literature as a function of reciprocal absolute temperature.

Note with the exception of the value reported by Gautelier *et al.* (2007) at 80 °C no dolomite solubility products have been reported for temperatures greater than 25 °C. Also show in Fig. 1 are dolomite solubility constants calculated using the equation of Langumir (1971) given by

$$-\log K_{sp^\circ-dol} = 17.0 + \frac{\Delta_r H^\circ_{298.15}}{4.576}\left(\frac{1}{T} - \frac{1}{298.15}\right) - \frac{\Delta_r C^\circ_{p298.15}}{1.987}\left[\frac{1}{2.303}\left(\frac{298.15}{T} - 1\right) - \log\frac{298.15}{T}\right] \quad (2)$$

which assumes that the heat capacity of this reaction at 298.15 K, $\Delta_r C^\circ_{p298.15}$ is constant below 25 °C. In Eqn. (2) T stands for temperature in K and $\Delta_r H^\circ_{298.15}$, the enthalpy of reaction (1) at 298.15 K was set equal to -38.854 kJ/mol (Langmuir, 1964). The $\Delta_r C^\circ_{p298.15}$ = 937.843 J/mol/K was calculated from the corresponding heat capacities of the ions in reaction (1) at 25 °C as reported by Criss and Coble (1964) and the heat capacity for dolomite of -157.842 J/mol/K

reported by Stout and Robie (1963). A summary of the thermodynamic properties of dolomite and the aqueous species present in reaction (1) are provided in Table 2.

Table 2. Values of standard state properties of dolomite and aqueous species involved in reaction (1) at 25 °C and 1 bar reported in the literature

Solid phase	$\Delta_f G^o_{298.15}$ **kJ/mol**	$S^o_{298.15}$ **J/mol/K**	$\Delta_f H^o_{298.15}$ **kJ/mol**	$C^o_{p\,298.15}$ **J/mol/K**	**Reference**
$CaMg(CO_3)_{2(cr)}$	-2161.7				Garrels *et al.* (1960)
				157.74	Stout and Robie (1963)
	-2121.9				Naumov *et al.* (1974)
	-2162.35	154.89	-2325.25		Berman (1988)
	-2161.7±1.1		-2324.5±1.1	157.53	Robie *et al.* (1978)/Hemingway and Robie (1994)
	-2163.4				Wagman *et al.* (1982)
	-2161.3±1.7	155.2±0.3	-2324.5±1.5	157.51	Robie and Hemingway (1995)
			-2330±3		Helgeson *et al.* (1978)/Chai and Navrotsky (1993)
	-2161.51	156.0	-2324.54		Holland and Powels (1998)
	-2147.82±2.2				Rock *et al.* (2001)
Aqueous species	$\Delta_f G^o_{298.15}$ **kJ/mol**	$S^o_{298.15}$ **J/mol/K**	$\Delta_f H^o_{298.15}$ **kJ/mol**	$C^o_{p\,298.15}$ **J/mol/K**	**Reference**
Mg^{2+}	-454.0	-138.1	-466.0	-22.3	Shock and Helgeson (1988)/Shock *et al.* (1997)
Ca^{2+}	-552.79	-56.48	-543.083	-30.96	Shock and Helgeson (1988)/Shock *et al.* (1997)
CO_3^{2-}	-527.98	-50.00	-675.24	-289.53	Shock and Helgeson (1988)

Stout and Robie (1963) determined the standard heat capacity and entropy of dolomite using calorimetric methods. These authors also calculated Gibbs free energy of formation ($\Delta_f G^o_{298.15}$) and enthalpy of formation ($\Delta_f H^o_{298.15}$) at 298.15 K from the analysis of dolomite decomposition data. Krupka *et al.* (1985) measured the heat capacity of dolomite at high temperatures using differential scanning calorimetry (DSC) and combined this data with

existing low temperature heat capacity reported by Stout and Robie (1963) and the high temperature relative enthalpy data reported by Southard (1941) and White (1919) to generate the following equation describing the heat capacity of dolomite as a function of temperature:

$$C_p^{\circ}{}_{(298\text{-}650K)} = 547.88 - 0.16759 \times T + 2.840 \times 10^{-6} \times T^{-2} - 6547.9\ T^{-0.5} + 7.7076 \times 10^{-5}\ T^{2},$$

where C_p° is in units of J/(mol.K). This equation yields a C_p° value of 157.51 J/mol/K at 298.15 K. Hemingway and Robie (1994) reported the enthalpy of formation of dolomite determined by HCl solution calorimetry at 27 °C acknowledging some problems that occurred during the experiments including CO_2 liberation in the calorimeter and the questionable crystallinity of the reference materials, which were assumed to be identical with the solid used to determine the enthalpies of formation. Moreover, the values of Navrotsky and Capobianco (1987) are in disagreement with those of Robie *et al.* (1978); this latter study noted that the solvent used in their acid solution measurements may not be consistent with the laws of dilute solutions.

Incongruent dissolution of initial solids has been reported in many experimentally based dolomite kinetic studies with a molar Ca/Mg concentration ratio of the departing divalent cations ranging between 2 and 6 (Debure *et al.*, 2013; Pokrovsky and Schott, 2001; Pokrovsky *et al.*, 2005; Zhang *et al.*, 2007). The lower hydration energy of Ca^{2+} compared to Mg^{2+} and the lower stability of Ca^{2+} at the dolomite/water interface could explain this preferential Ca release (Busenberg and Plummer, 1982; Pokrovsky and Schott, 2001; Zhang *et al.*, 2007). In contrast, based on Atomic Force Microscopy (AFM) observations, Urosevic *et al.* (2012) suggest that dolomite dissolves via a dissolution-precipitation reaction at all pH and at close to equilibrium conditions with the formation of nesquehonite as a Mg-rich surface precipitate. According to these authors, this precipitate would redissolve as dissolution continues.

3. Materials and methods

3.1 Dolomite sample

Dolomite crystals from Sainte Colombe (Aude, France; hydrothermal origin) were hand crushed with mortar and pestle, dry sieved, and ultrasonically cleaned in pure ethanol to obtain the 50 and 100 µm size fraction. A magnetic separation of the resulting material was performed to remove minor amounts of magnetite. Scanning Electron Microscope (SEM) images, obtained using a JEOL JSM-6360 LV microscope of the resulting dolomite are shown in Fig. 2. The image shows the powder to be consist of only dolomite and free of adhering fine particles. The specific surface area of the prepared dolomite was determined to be 0.0804 m^2/g m^2/g by multipoint krypton adsorption according to the BET method (Brunauer *et al.*, 1938) using a Quantachrome Gas Sorption system.

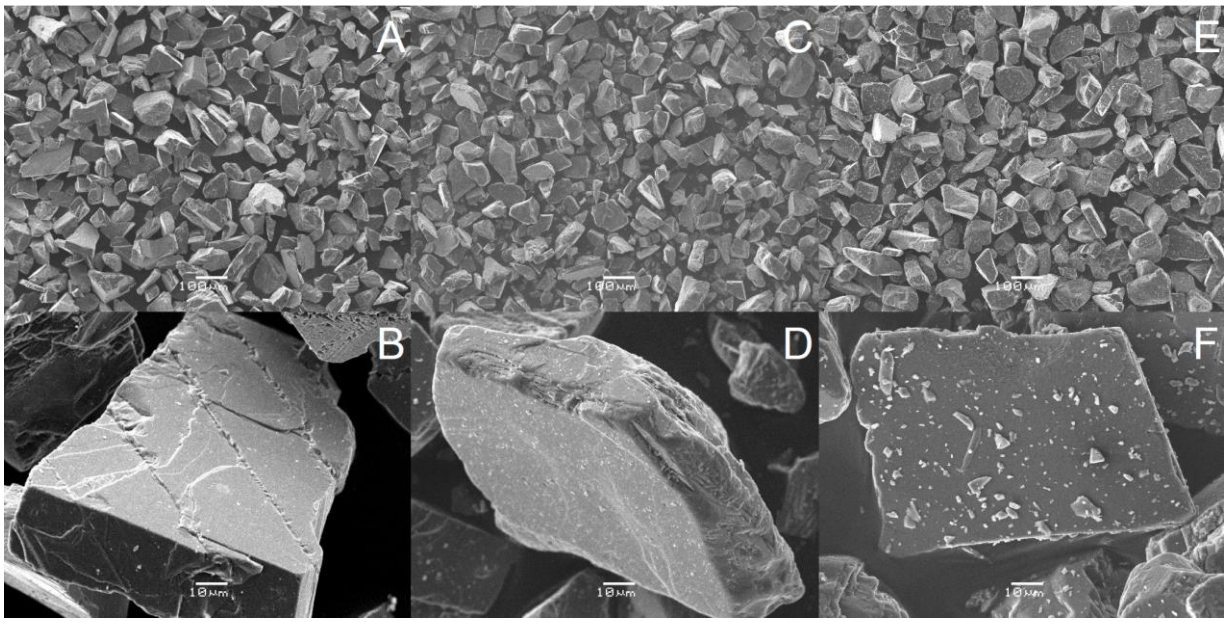

Figure 2: Scanning electron micrographs of (A, B) the initial Sainte Colombe dolomite seed material, (C,D) this material after its use in dissolution experimental series 3, and (E,F) this material after its use in the dissolution-reprecipitation experimental series 5.

The mineralogical composition of the dolomite seed material was determined by electron microprobe analysis and is reported in Table 3**.** The purity of this dolomite was verified via X-ray diffraction using an INEL CPS-120 diffractometer with Co Kα-radiation, λ=1.78897 Å and a graphite monochromator. Scans were performed from 1 to 110º 2θ at 0.09º/min and a step size of 0.029º. This analysis demonstrates the cation-ordered structure of this dolomite.

Table 3: Chemical composition of the initial Sainte Colombe dolomite seeds before the experiments and following its reaction in selected experimental series

	Initial Sainte Colombe dolomite seeds	Dolomite recovered from experimental series 2	Dolomite recovered from experimental series Run 5
CaO	34.35	34.40	34.60
MgO	22.72	22.86	23.00
FeO	0.0122	0.0101	0.0126
MnO	0.0075	0.0088	0.0090
TiO_2	0.0092	0.0071	0.0083
Cr_2O_3	0.0026	0.0039	0.0053
Al_2O_3	0.0033	0.0070	0.0061
SiO_2	0.0122	0.0064	0.0040
Na_2O	0.0037	0.0063	0.0051
K_2O	0.0017	0.0034	0.0034
calculated CO_2	42.89	42.69	42.35
chem. formula	$Ca_{1.04}Mg_{0.96}(CO_3)_2$	$Ca_{1.04}Mg_{0.96}(CO_3)_2$	$Ca_{1.04}Mg_{0.96}(CO_3)_2$

3.2 Hydrogen-electrode concentration cell (HECC)

Dolomite solubility was measured from 50 to 175 °C in aqueous 0.1 mol/kg NaCl solutions using a hydrogen electrode concentration cell (HECC). This cell has been described in detail by Bénézeth *et al.* (2007, 2009, and 2011). Thhis cell is unique in its ability to measure in situ pH at a very high precision at temperatures up to ~300 °C, a crucial parameter

to define carbonate speciation and thus its solubility constants. The uncertainties of pH determined in this cell are estimated to be 2%. Additionally the cell design avoids any potential for the fluid to equilibrate with atmospheric CO_2.

Experiments in this study were performed in several series of experiments performed on a single dolomite seed material. Each experimental series was initiated by placing the initial fluid with a pH_m of ~3 and ~3 g of the initial dolomite seeds into the cell. The initial conditions of all experimental series are listed in Table 4. The cell was then heated to the temperature of interest. Once the cell attained thermal equilibrium, fluid samples were withdrawn over time. During each sampling approximately 5 ml of fluid was withdrawn via an Hastelloy valve through a platinum dip tube fitted with a porous Teflon frit (3 μm), and then through a polyvinylidene Acrodisc LC13 porosity filter with a 0.2 μm mesh size.

Table 4. Stoichiometric molal compositions of starting solutions for HECC experiments

Experimental series #	*T* (°C) range investigated	Reference and test cell *m*(HCl) x10^3	*m*(NaCl)
2	100-150-100	2.5001	0.0975
3	175-50	2.5001	0.0975
4	175-125	2.5001	0.0975
5	150-100-150	2.5001	0.0975
6	125-175	2.4996	0.0975

Fractions of the each fluid sample were devoted to analyses of dissolved magnesium and calcium, as well as to determine the total dissolved inorganic carbon (TDIC). Steady-state fluid compositions were attained within few weeks (at temperature $T \geq 100$ °C); nevertheless samples were taken during longer time intervals to verify attainment of steady state (see Table 6). The cell temperature was subsequently decreased allowing the system to again approach

equilibrium from under-saturation. During the course of some runs (5 and 6), the temperature was raised (from 100 to 150 °C and from 125 to 175 °C, respectively) allowing the system to approach equilibrium from over-saturation.

3.3 Fluid Analyses

Fluid samples were analyzed for magnesium, calcium, and total dissolved inorganic carbon (TDIC). Mg and Ca were analyzed using a Perkin Elmer AAnalyst 400 Atomic Absorption Spectrometer (AAS) with an uncertainty of ±2% and a detection limit of 2×10^{-7}. These analyses were calibrated using Mg and Ca standard solutions having concentrations of 0.1 to 0.6 ppm and 0.5 to 5 ppm, respectively; these standard solutions were prepared with the same matrixes as the experiments.

TDIC was analyzed using a LI-820 (LICOR Inc.) non dispersive infra-red (NDIR) CO_2 gas analyzer. This method is based on the measurement of the IR energy absorbed by the CO_2 extracted from a sample by acidification along an optical path, compared to a reference signal (see Bénézeth *et al.*, 2011 for the details of the technique). The TDIC concentration is calculated using calibrations curves; the calibration curves were created by analyzing a suite of standard solutions prepared from dried reagent grade Na_2CO_3 and $NaHCO_3$. Combining this TDIC with in situ pH measurements allows the calculation of the aqueous carbonate speciation at the temperature of the experiments using the apparent dissociation constants (Q) of the following reactions:

$$CO_{2(aq)} + H_2O = HCO_3^- + H^+ \quad (3)$$

and

$$HCO_3^- = H^+ + CO_3^{2-} \quad (4)$$

in aqueous 0.1 mol/kg NaCl solutions. The values of Q for reactions 3 and 4 were taken from Patterson *et al.* (1982 and 1984, respectively). The uncertainty of the analyses performed in this study is generally lower than 5% with a TDIC with a detection limit of 10^{-3} to 10^{-5} mol/kg depending upon the length of the optical bench (5 or 14 cm, respectively).

4. Experimental results

4.1 Determination of dolomite solubility product

The results of the solubility experiments performed in the HECC are summarized in Table 5. The apparent solubility products for reaction (1), defined as $Q_{sp\text{-}dol} = [Mg^{2+}][Ca^{2+}][CO_3^{2-}]^2$, are reported in Table 6. The ionic strength and the carbonate speciation reported in these tables were calculated iteratively from the measured pH_m, and total Mg, Ca, and TDIC concentrations, reported in Table 5.

Table 5. Steady-state fluid concentrations in all dolomite solubility experiments performed in this study.

Experiment #	***T*** (°C)	**-log[H^+]^a** measured *in situ*	**log[Mg^{2+}]^a** measured by AAS	**log[Ca^{2+}]^a** measured by AAS	**[TDIC]^a** measured by NDIR x10^3	**[CO_3^{2-}]^a** x10^7	**Equilibrium Time** (hours)
2.1	*100.8*	*7.024*	*-3.042*	*-2.932*	*1.430*	*37.67*	*744*
2.2*	*125.7*	*6.641*	*-3.128*	*-2.951*	*0.946*	*8.124*	*936*
2.3*	*150.8*	*6.107*	*-3.219*	*-2.926*	*0.763*	*0.829*	*720*
2.4**	*101.4*	*6.258*	*-3.051*	*-2.842*	*1.750*	*5.161*	*624*
3.1	175.5	6.443	-3.189	-3.025	0.658	1.674	281
3.2	148.6	6.460	-3.141	-2.999	0.755	2.996	498
3.3	125.1	6.532	-3.078	-2.971	1.061	6.578	427
3.4	99.8	6.666	-2.992	-2.942	1.454	14.76	664
3.5	75.9	6.845	-2.925	-2.885	2.044	32.35	760
3.6	50.6	7.197	-2.814	-2.818	2.957	92.44	1128
4	174.6	6.537	-3.212	-3.026	0.525	1.908	144
5.1	152.1	6.416	-3.145	-3.007	1.072	3.508	384
5.2	100.5	6.626	-2.964	-2.878	2.225	20.20	528

5.3*	152.2	6.260	-3.127	-3.013	0.984	1.849	432
6.1	124.7	6.721	-3.134	-2.999	0.781	8.468	1320
6.2*	175.1	6.425	-3.237	-3.029	0.413	0.997	300
6.3**	125.0	6.583	-3.176	-2.984	0.691	4.994	227
6.4**	**77.6**	**6.863**	**-3.057**	**-2.885**	**1.354**	**22.22**	**224**

[a] Molal concentrations in the experimental solutions
*re-increasing temperature, approaching equilibrium from supersaturation, **re-decreasing temperature
In italic, a run that did not behave correctly, not included in the fit.
Bold: steady state not yet attained

The equilibrium constant for reaction (1) $K_{sp°\text{-}dol}$, can be obtained from the reaction product using

$$K_{sp°\text{-}dol} = Q_{sp\text{-}dol} (\gamma_{Mg^{2+}})(\gamma_{Ca^{2+}}) (\gamma_{CO_3^{2-}})^2 \quad (5)$$

where γ_i defines the activity coefficient of the i^{th} aqueous species. The mean stoichiometric activity coefficients were derived from the Meissner equation (Lindsay, 1989) ($\gamma_{|z|} = \gamma_{\pm(NaCl)}^{z^2}$; *cf.* Bénézeth *et al.*, 2011 for more details). These latter values were calculated from Archer (1992) and are given in Table 6.

Table 6. Dolomite apparent solubility products, $Q_{sp\text{-}dol}$, ionic strengths, I, activity coefficients, $\gamma_{\pm(NaCl)}$, and the equilibrium constant for reaction (1), $K_{sp°\text{-}dol}$, calculated for all experiments performed in this study

Run #	T (°C)	$\log_{10}Q_{sp\text{-}dol}$	I mol·kg^{-1}	$\gamma_{\pm(NaCl)}$	§$\log_{10}K_{sp°\text{-}dol}$
2.1	*100.8*	*-16.82*	*0.1038*	*0.7430*	*-18.89 ± 0.3*
2.2	*125.7*	*-18.26*	*0.1036*	*0.7278*	*-20.47 ± 0.3*
2.3	*150.8*	*-20.31*	*0.1035*	*0.7091*	*-22.69 ± 0.3*
2.4	*101.4*	*-18.47*	*0.1046*	*0.7420*	*-20.54 ± 0.3*
3.1	175.5	-19.77	0.1019	0.6895	-22.35 ± 0.3
3.2	148.6	-19.19	0.1030	0.7114	-21.55 ± 0.3
3.3	125.2	-18.41	0.1034	0.7099	-20.62 ± 0.3
3.4	99.8	-17.60	0.1041	0.7436	-19.66 ± 0.3
3.5	75.9	-16.79	0.1051	0.7555	-18.74 ± 0.4
3.6	50.6	-15.70	0.1067	0.7654	-17.56 ± 0.4

4	174.6	-19.68	0.1025	0.6898	-22.26 ± 0.3
5.1	152.1	-19.06	0.1029	0.7086	-21.46 ± 0.3
5.2	100.5	-17.23	0.1048	0.7426	-19.30 ± 0.3
5.3*	152.2	-19.61	0.1031	0.7085	-22.00 ± 0.3
6.1	125.7	-18.28	0.1029	0.7287	-20.48 ± 0.3
6.2*	175.1	-20.27	0.1027	0.6891	-22.86 ± 0.3
6.3**	125.0	-18.76	0.1029	0.7284	-20.96 ± 0.3
6.4**	**77.6**				**-19.19 ± 0.4**

§ Uncertainties estimated from the combined experimental uncertainties.
* equilibrium approached from supersaturation, ** equilibrium approached from undersaturation
Bold: steady state not yet attained.

The logarithms of the equilibrium constants listed from Table 6 are shown in Figure 3 as a function of reciprocal temperature.

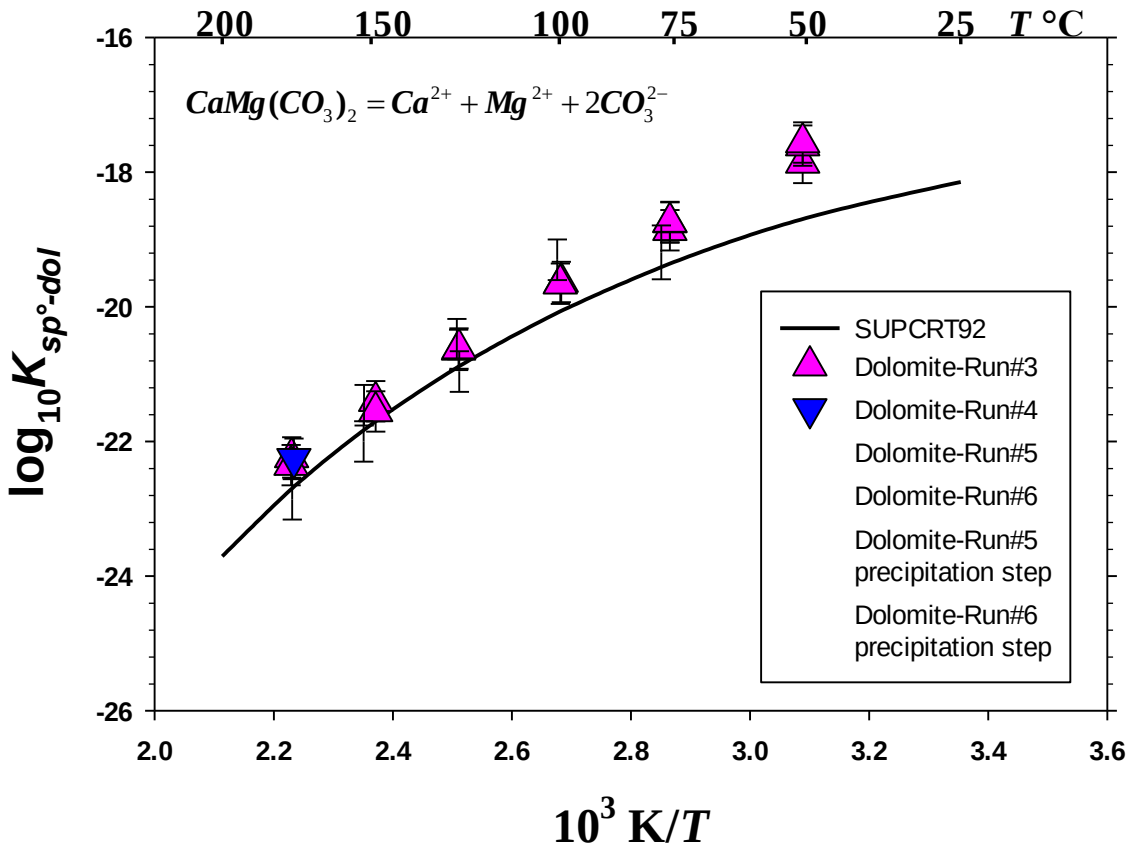

Figure 3: All dolomite equilibrium constants measured in this study plotted as a function of reciprocal temperature.

Note that all solubilities determined during experimental series 3 which are shown as pink triangles in Figure 3 were approached only from under-saturation, by first starting at 175 °C and then decreasing the temperature successively to 50 °C. This experimental series took 6 months to be completed. Experimental series 4 was performed only at 175 °C; the solubilities obtained in this series are shown as blue triangles in Figure 3. The first two experiments in series 5 determined dolomite solubilities at 150 and 100 °C from undersaturation; these solubilities are shown as green circles in Figure 3. Once steady-state was attained at 100 °C, the temperature was raised to 150 °C, allowing the approach of equilibrium from super-saturation. Steady state was achieved in 18 days in this experiment. The resulting solubility of experiment 5.3 is shown as a green circle/hourglass symbol in Fig. 3. The close match between the measured solubilities obtained at 150 °C from both under and supersaturated fluids demonstrates that the reversibility of equilibrium was achieved in this experimental series, even though the log $K_{sp°\text{-}dol}$ obtained is slightly lower than that observed during experiment 5.1 and experiment 3.2. Similarly the result of experiment 6.2, shown as cyan squares in Fig. 3, was obtained from supersaturation conditions at 175 °C. As for experiment 5.3, the log $K_{sp°\text{-}dol}$ obtained from experiment 6.2 performed at 175 °C approaching equilibrium from supersaturation is ~0.5 log units lower than that obtained by approaching equilibrium from undersaturation.. Note these lower log $K_{sp°\text{-}dol}$ values suggest that the dolomite which precipitated during the supersaturated experiments is more stable than the initial dolomite being dissolved during the undersaturated experiments.

The composition of the precipitated dolomite during the experiments can be deduced from the temporal evolution of the reactive fluids. Fig. 4 show this temporal evolution of TDIC and aqueous Ca and Mg for experimental run 5. Molar calcium to magnesium ratios are

close to unity at all investigated temperatures and this ratio is kept constant during the dissolution and reprecipitation experiments. Similarly, the amount of TDIC was released during the initial dissolution at 150 and 100 °C decreases back to its former concentration during as dolomite precipitated upon increasing temperature to 50 °C. These observations are consistent with the stoichiometric dissolution and precipitation of dolomite.

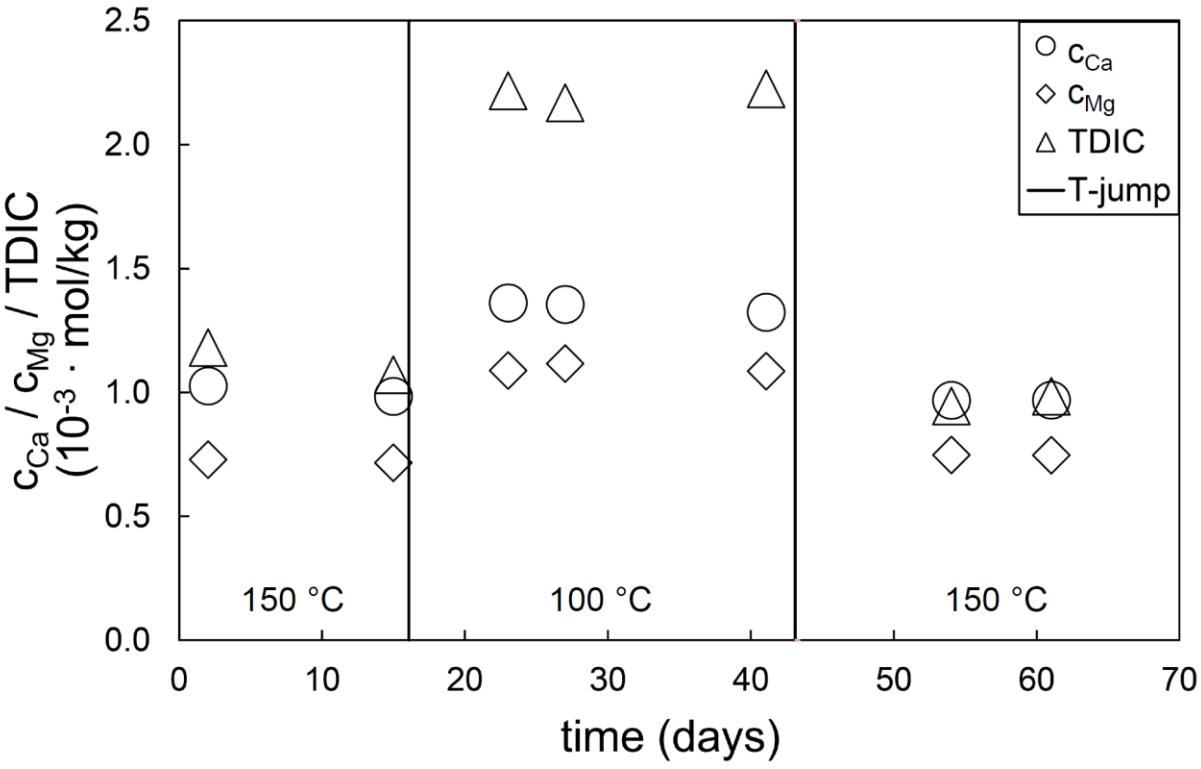

Figure 4: Temporal evolution of TDIC and aqueous Ca and Mg concentration of durig experimental series 5. Uncertainties in the concentration measurements are within the size of the symbols. Note that the reactor temperature was first decreased from 150 to 100 °C and then increased back to 150 °C provoking dolomite precipitation.

Analyses performed on the solids recovered after all of the experimental series show these samples to be free of all carbonate phases other than of dolomite. Electron microprobe analysis of the solids recovered after dissolution and precipitation in experimental series 2 and 5 show these to have an identical composition to that of the initial dolomite powder (see Table 3). X-ray diffraction analysis of the solids recovered from series 5 suggested the presence of

traces of phyllosilicates (muscovite and chlorite). The presence of trace muscovite was also detected by energy-dispersive X-ray spectroscopy in the solids recovered from experimental series 2. The presence of these trace impurities, however, has negligible influence on the solubility product constants measured in this study.

Scanning electron micrographs taken of the solids recovered after series 3 reveals some dissolution features including rounded grain edges (compare Figures 2A and B with 2C and D). The quenched solids retrieved directly after experimental series 5 exhibits mineral growth on the dolomite seed material surfaces (see Figure 2E and F). Electron backscattering verifies additionally that these growths have the same chemical composition as the dolomite seed material. Moreover X-ray photoelectron spectroscopy (XPS) analysis was performed on the solids recovered from series 5 and the unreacted Sainte Colombe dolomite powder for comparison. The XPS analyses were performed with a 700x300 µm spot size thus averaging the analysis over several grains. Atomic percentages obtained from these measurements were close to stoichiometric dolomite revealing a calcium to magnesium ratio of 1.00 and 0.97 for both the initial Sainte Colombe dolomite and the solids recovered after series 5. Significant differences, however, are evident in the binding energies (BE) and the full width half maximum (FWHM) of the surface atoms between the unreacted dolomite surface and the samples recovered after series 5 (see Table 7). The binding energies of the surface atoms of the solids recovered after series 5 are slightly, but systematically shifted to higher values indicating a distinct chemical environment. The BE-values of the grains recovered after series 5 are similar to what is normally observed for calcite (reference). The significantly higher FWHM-values suggest a less ordered and increased coordination number of the surface atoms in the solids recovered after series 5.

Table 7: Binding energies (BE in eV) and full width half maximum (FWHM in eV) for C in CO_3, O in CO_3, Ca, and Mg obtained from XPS analysis.

	C 1s (CO_3)		O 1s (CO_3)		Ca 2p3/2		Mg 2s	
	BE	FWHM	BE	FWHM	BE	FWHM	BE	FWHM
Initial dolomite	289.8	1.27	531.6	1.44	347.3	1.32	89	1.67
Post series 5	290.2	1.68	531.9	1.66	347.6	1.68	89.3	1.91

XPS measurements revealed additional differences between these two samples. In contrast to the initial dolomite, the surfaces of the post series 5 solids were prone to increasing X-ray damage with increasing exposure time exemplified by the development of secondary Mg 2s peaks at higher binding energies and their increasing intensity with increasing X-ray exposure time. This increased fragility in response to X-ray exposure of the post series 5 sample may indicate some sort of lattice-misfits of the grown phase. Moreover, the intensity ratios of Mg 1s to Mg 2s peaks differ significantly between the initial and post series 5 solids. Due to the lower kinetic energy of Mg 1s compared to Mg 2s photoelectrons, the latter may travel further into the solid. Hence, the observed differences in these ratios could either mean a depletion of Mg^{2+} in the lower regions of the growth layer, an enrichment of Mg^{2+} in the uppermost layer, and/or a combination of both.

4.2 Retrevial of dolomite thermodynamic properties

Measured dolomite solubility product constants in this study are closely consistent with

$$\mathrm{Log}_{10}\, K_{\mathrm{sp°\text{-}dol}} = a + b/T\,(\mathrm{K}) + cT\,(\mathrm{K}). \quad (6)$$

where a, b, and c are regression coefficients. Eq. (6) is consistent with

$$\Delta G_r^0 = -R \ln(10)\{aT + b + cT^2\} \quad (7)$$

which can be differentiated with respect to T to obtain these expressions of the reaction (1) enthalpy and heat capacity:

$$\Delta H_{\mathrm{r}}^{\mathrm{o}} = R \ln(10)\{-b+cT^2\} \quad (8)$$

$$\Delta C_{p,\mathrm{r}}^{\mathrm{o}} = 2\, RT \ln(10)\, c \quad (9)$$

A first fit of our solubility product constants took account of all the experimental data with their respective errors as reported in Table 6. The parameters and thermodynamic values obtained from this regression are listed in Table 8. This regression yielded the dashed blue curve in Figure 5. A second fit was made by fixing $\mathrm{Log}_{10}\, K_{\mathrm{sp°\text{-}dol}}$ to -17.2 at 25 °C. The result of this second fit is shown as a dashed green curve in Figure 5. A third fit was made by fixing $\Delta_r C_p^{\mathrm{o}}$ to -789.832 J/mol/K at 25 °C with c = -0.06919; this heat capacity is consistent with the dolomite isobaric heat capacity reported by Robie and Hemingway (1995). The result of this third fit is shown as a red dashed curve in Figure 5. The parameters corresponding to these 3 fits are listed in Table 8.

Table 8. Parameters for use in equations 6 to 9 describing the thermodynamic properties of the dolomite solubility reaction as a function of temperature from 25 to 200 °C.

$\mathrm{Log}_{10}K_{\mathrm{sp°\text{-}dol}} = a + b/T\,(\mathrm{K}) + cT\,(\mathrm{K})$	a	b	C	$\mathrm{Log}_{10}K_{\mathrm{sp°\text{-}dol}}$ 25°C	$\Delta_f \mathrm{G}^{\mathrm{o}}_{298.15}$ kJ/mol	$\Delta_f \mathrm{H}^{\mathrm{o}}_{298.15}$ kJ/mol	$Cp^{\mathrm{o}}_{298.15}$ J/mol/K
Fit of all the experimental data	-16.4386	2133.9973	-0.02415	-16.48*	-2156.81	-2277.57	-356.63
Fit of all the experimental data - fixed 25°C	0.7692	-940.5699	-0.04393	*-17.20 (fixed)* *-17.00**	-2159.89	-2302.77	-130.83
Fit of all the experimental data - fixed $\Delta C_{p,\mathrm{r}}^{\mathrm{o}}$	18.4224	-4533.0567	*-0.06919*	-17.41*	-2162.11	-2328.56	157.54

In italic: fixed value in the fit

*calculated using Eq. 6 and the fitting parameters

The parameters listed in Table 8 can be used together with Eqs. (7)-(9) to generate the thermodynamic properties of reaction (1) at 25 °C. Combining these values with the thermodynamic parameters for Mg^{2+}, Ca^{2+} and CO_3^{2-} from Shock *et al.* (1997) (see Table 2), we obtained the dolomite thermodynamic properties at 25 °C and 1 bar as listed in Table 8.

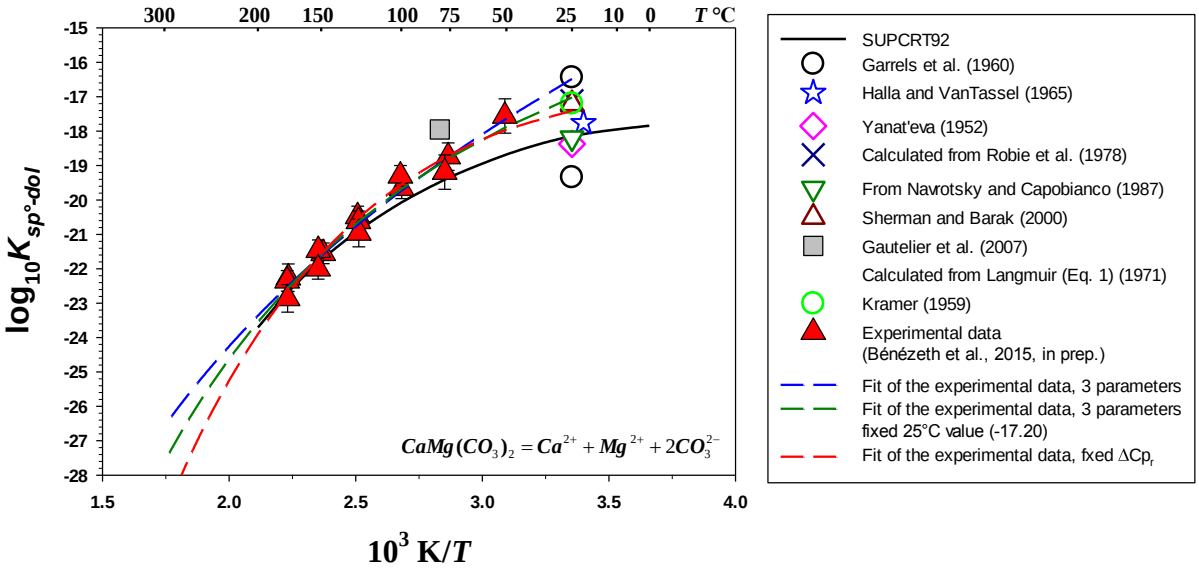

Figure 5: Summary of dolomite solubility products as a function of reciprocal temperature. A description of the various fit curves is provided in the text.

4. Discussion

This study is the first to systematically measure dolomite solubility at elevated temperatures. This study was only possible due to the precise in situ pH measurements made using the hydrogen cell reactor. Furthermore, the reported experiments bracket equilibrated dolomite from both undersaturated and supersaturated conditions and thereby strongly constraining the equilibrium constants of reaction (1). The obtained equilibrium constants at 125 to 150 °C are nearly identical to SUPCRT92, but then to be as much as 1.8 orders of magnitude depending lower at 50 °C. Since reaction (1) involves four aqueous species it seems

reasonable that dolomite is about 0.4 log units more soluble than predicted by the equilibrium constants provided by SUPCRT92 at 50 °C.

Our results suggest that the dolomite solubility product constant at 25 °C is in the range -16,5 to -17.2. The good agreement of our data with the experiments of Kramer (1959) and Sherman and Barak (2000), the later study performed experiments that lasted two years. These values are also in excellent agreement with geological observations; Hsu (1963) reported a solubility constant of $10^{-17.2}$ determined from the composition of groundwaters sampled from dolomite aquifers. Additionally, all these results are in good agreement to the thermodynamic data derived from solution calorimetry published by Robie *et al.* (1978)

5. Conclusion

Experimental evidence on the solubility of dolomite has been controversial and few dolomite solubility data are available at elevated temperature. This study was the first to systematically measure dolomite solubility at elevated temperatures. Application of these results will likely improve our ability to quantify subsurface carbon storage and provide insight into the origin of the dolomite problem.

In this study, dolomite solubility was measured from 50 to 175 °C. Equilibrium was approached both from under-saturation and super-saturation demonstrating its reversibility. From the regression of our measured dolomite solubility constants as a function of temperature we generated the thermodynamic properties of dolomite as well as equations and parameters describing the dolomite solubility product from 25 to 300 °C. Calculated 25 °C dolomite consistent with most of the previous data but significantly higher than that generated from SUPCRT92, or that reported by Navrotsky and Capobianco (1987). The close agreement with previous thermodynamic data obtained from calorimetric measurements and high *P*-high *T*

phase equilibrium studies can be made by only taking into account the dolomite heat capacity reported by Robie and Hemingway (1995).

Acknowledgments

Michel Thibaut, Alain Castillo, Thierry Aigouy, Philippe de Parseval and Carole Causserand (GET) are thanked for their assistances with XRD, BET, SEM, ion probe and chemical analyses, respectively.

References

Anatao S.M., Mulder W.H., Hassan I., Crichton W.A. and Parise J.B. (2004) Cation disorder in dolomite, $CaMg(CO_3)_2$, and its influence on the aragonite + magnesite ↔ dolomite reaction boundary. *American Mineralogist*, **89**, 1142-1147.

Archer D.G. (1992). Thermodynamic properties of the NaCl + H_2O system. II. Thermodynamic properties of NaCl(aq), $NaCl{\cdot}2H_2O$(cr), and phase equilibria. *J. Phys. Chem. Ref. Data* **21**,

Arvidson R.S. and Mackenzie F.T. (1999) The dolomite problem: Control of precipitation kinetics by temperature and saturation state. *Am. J. Sci.,* **299**, 257-288.

Barnes J. and Back W. (1964) Dolomite solubility in ground water. *U.S. Geol. Surv. Prof. Paper* **475-D**, 179-180.

Bénézeth P, Saldi G, Dandurand J-L and Schott J. (2011) Experimental determination of the solubility product of magnesite at 50 to 200°C. *Chem. Geol.*, **286**, 21-31.

Bénézeth P., Dandurand J.-L. and Harrichoury J.-C. (2009). Solubility product of siderite ($FeCO_3$) as a function of temperature (25-250°C). *Chem. Geol.* **265**, 3-12.

Bénézeth P., Palmer D.A., Anovitz L.M. and Horita J. (2007). Dawsonite synthesis and reevaluation of its thermodynamic properties from solubility measurements: implications for mineral trapping of CO_2. *Geochim. Cosmochim. Acta* **71**, 4438-4455.

Berman R.G. (1988). Internally consistent thermodynamic data for minerals in the system Na_2O-K_2O-CaO-MgO-FeO-Fe_2O_3-Al_2O_3-SiO_2-TiO_2-H_2O-CO_2. *Journal of Petrology* **29**, 445-522.

Chai L. and Navrotsky A. (1993) Thermochemistry of carbonate- pyroxene equilibria. *Contrib. Mineral. Petrol.*, **114**,139–147.

Criss C.M. and Cobble J.W. (1964) The thermodynamic properties of high temperature aqueous solutions. V. The calculation of ionic heat capacities up to 200°. Entropies and heat capacities above 200°C. *J. Amer. Chem. Soc.*, **86**, 5390-5393.

Debure M., Frugier P., De Windt L. and Gin S. (2013) Dolomite effect on borosilicate glass alteration. *Appl. Geochem.*, **33**, 237-251

Garrels R., Thompson M.E. and Siever R. (1960) Stability of some carbonates at 25°C and one atmosphere total pressure. *Am. J. Sci.*, **258**, 402–418.

Garrels R.M., Thompson M.E. and Siever R. (1961) Control of carbonate solubility by carbonate complexes. *Am. J. Sci.*, **259**, 24-45.

Gautelier M., Schott J. and Oelkers E.H. (2007) An experimental study of dolomite dissolution rates at 80ºC as a function of chemical affinity and solution composition. *Chem. Geol.*, **242**, 509–517.

Halla V.F. and Van Tassel R. (1965) Auflosungserscheinungen bei erdalkalikarbonaten I. (Dissolution phenomena of alkaline earth aquacarbonates) *Radex-Rundschau* **4**, 595–599 (in German).

Helgeson H.C., Delany J.M., Nesbitt H.W. and Bird D.K. (1978) Summary and critique of the thermodynamic properties of rock-forming minerals. *Am. J. Sci.*, **278A**, 44–51.

Hemingway B.S. and Robie R.A.(1994) Enthalpy and Gibbs energy of formation of dolomite, $CaMg(CO_3)_2$, at 298.15 K from HCl solution calorimetry. *U.S. Geological Survey, open-file report 94-575*.

Holland T.J.B. and Powell R. (1990) An enlarged and updated internally consistent thermodynamic dataset with uncertainties and correlations: The system K_2O–Na_2O–CaO–MgO–MnO–FeO–Fe_2O_3–Al_2O_3–TiO_2–SiO_2–C–H_2–O_2. *J. Metamorphic Geol.*, **8**, 89–124.

Hsu K.J. (1963) Solubility of dolomite and composition of Florida groundwaters. *J. Hydrol.* **1**,288–310.

Johnson J.W., Oelkers E.H. and Helgeson H.C. (1992). SUPCRT92 - A software package for calculating the standard molal thermodynamic properties of minerals, gases, aqueous species, and reactions from 1 to 5000 bar and 0 to 1000°C. *Computers & Geosciences* **18**, 899-947.

Kramer J.R. (1959) Correction of some earlier data on calcite and dolomite in sea water. *J. Sediment. Petrol.*, **29**, 465–467.

Krupka K.M., Hemingway B.S., Robie R.A. and Kerrick D.M. (1985) High-temperature heat capacities and derived thermodynamic properties of anthophyllite, diopside, dolomite, enstatite, bronzite, talc, tremolite, and wollastonite. *Am. Mineral.*, **70**, 261–271.

Land L.S. (1998) Failure to precipitate dolomite at 25 °C from dilute solution despite 1000-fold oversaturation after 32 years. *Aquatic Geochemistry*, **4**, 361-368.

Langmuir D. (1971) The geochemistry of some carbonate ground waters in central Pennsylvania. *Geochim. Cosmochim. Acta*, **35**, 1023–1045.

Langmuir D. (1964) Stability of carbonates in the system CaO-MgO-CO_2-H_2O. Ph.D. Thesis, Harvard University.

Lindsay Jr. W.T. (1989). Chemistry of steam cycle solutions: principles. In: Cohen, P. (Ed.),

The ASME handbook on water technology for thermal power plants. The American Society of Mechanical Engineers, New York, pp. 341–544. Chapter 7.

Lippmann F. (1973) *Sedimentary Carbonate Minerals*. Springer-Verlag, New-York.

Navrotsky A. and Capobianco C. (1987) Enthalpies of formation of dolomite and magnesian calcites. *Am. Mine.*, **75**, 782-787.

Patterson C.S., Slocum G.H., Busey R.H. and Mesmer R.E. (1982). Carbonate equilibria in hydrothermal systems: first ionization of carbonic acid in NaCl media to 300°C. *Geochim. Cosmochim. Acta* **46**, 1653–1663.

Patterson C.S., Busey R.H. and Mesmer R.E. (1984). Second ionization of carbonic acid in NaCl media to 250 °C. *J. Solution Chem.* **13**, 647-661.

Plummer L.N. and Busenberg E. (1982) The solubilities of calcite, aragonite and vaterite in CO_2–H_2O solutions between 0 and 90°C, and an evaluation of the aqueous model for the system $CaCO_3$–CO_2–H_2O. *Geochim. Cosmochim. Acta*, **46**,1011–1040.

Pokrovsky O.S. and Schott J. (2001). Kinetics and mechanism of dolomite dissolution in neutral to alkaline solution revisited. *Am. J. Sci.*, **301**, 597–626.

Pokrovsky O.S., Golubev S.V. and Schott J. (2005). Dissolution kinetics of calcite, dolomite and magnesite at 25°C and 0 to 50 atm pCO_2. *Chem. Geol.*, **217**, 239–255.

Robie R.A. and Hemingway B.S. (1995). Thermodynamic properties of minerals and related substances at 298.15 K and 1 bar (105 Pa) pressure and at higher temperatures. *U.S. Geol. Survey Bull.*, **2131**, p.461.

Robie R.A., Hemingway B.S. and Fisher J.R. (1978) Thermodynamic properties of minerals and related substances at 298.15K and 1 bar (10^5 Pascals) pressure and at higher temperatures. *U .S. Geological Survey Bulletin 1452*. Reprinted with corrections, 1979.

Rock P.A., Mandell G.K., Casey W.H. and Walling E.M. (2001) Gibbs energy of formation of dolomite from electrochemical cell measurements and theoretical calculations. *Am. J. Sci.*, **301**, 103–111.

Sherman L.A. and Barak P. (2000) Solubility and dissolution kinetics of dolomite in Ca-Mg-HCO_3/CO_3 solutions at 25°C and 0.1 MPa carbon dioxide. *Soil Sci. Soc. Am. J.*, **64**, 1959-1968.

Shock E.L. and Helgeson H.C. (1988). Calculation of the thermodynamic and transport properties of aqueous species at high pressures and temperatures: correlation algorithms for ionic species and equation of state predictions to 5kb and 1000°C. *Geochim. Cosmochim. Acta* **52**, 2009-2036.

Shock E.L., Sassani D.C., Willis M. and Sverjensky D.A. (1997). Inorganic species in geologic fluids: Correlations among standard molal thermodynamic properties of aqueous ions and hydroxide complexes. *Geochim. Cosmochim. Acta* **61**, 907-950.

Southard I.C. (1941) A modified calorimeter for high temperatures. The heat content of silica, wollastonite and thorium dioxide above 25°C. *J. Amer. Chem. Soc.*, **63**, 3142-3146.

Stout J.W. and Robie R.A. (1963). Heat capacity from 11 to 300 K, entropy, and heat of formation of dolomite. *J. Phys. Chem*. **67** (11), 2248-2252.

Urosevic M., Rodriguez-Navarro C., Putnis C.V., Cardell C., Putnis A. and Ruiz-Agudo E. (2012) In situ nanoscale observations of the dissolution of {$10\bar{1}4$} dolomite cleavage surfaces. *Geochim. Cosmochim. Acta* **80**, 1-13.

Usdovski E. (1994) Synthesis of dolomite and geochemical implications. *In* Dolomites: A Volume in Honour of Dolomieu, B. Purser et al., Ed., pp. 345–360, Blackwell Sci. Publ, Oxford, UK, 1994.

Yanat'eva O.K. (1952) Solubility of dolomite in water salt solutions. *Izvestiya Sektora FkhA Akademii Nauk SSSR,* **20**, 252-268 (In Russian).

Wagman D.D., Evans W.H., Parker V.B., Schumm R.H., Halow I., Bailey S.M. Churney K.L. and Nuttail R.L. (1982). The NBS tables of chemical thermodynamic properties: selected values for inorganic and C_1 and C_2 organic substances in SI units. *J. Chem. Ref. Data* **11** supplement n. 2, 392 pp.

White W.P. (1919) Silicate specific heats. Second series. *Amer. J. Sci.*, XLVII, 1-43.

Zhang R., Hu S., Zhang X. and Yu W. (2007) Dissolution kinetics of dolomite in water at elevated temperatures. *Aq. Geochem.*, **13**, 309–338.